The Energy Landscape of a Fluorite-Structured Superionic Conductor†

Angus Gray-Weale* and Paul A. Madden

Physical and Theoretical Chemistry Laboratory, University of Oxford, South Parks Road, OX1 3QZ, U.K.

Received: December 28, 2003; In Final Form: February 9, 2004

In a recent paper, we described similarities between the superionic transition in certain crystals and the glass transition in fragile, supercooled liquids. We now examine the underlying energy landscapes of the fluorides of lead(II) and calcium, by minimizing the potential energy from configurations along molecular-dynamics trajectories. The resulting inherent structures are characterized by the number of defects they contain and the interactions of these defects. We propose a simple explanation for the clustering of these defects, related to the lattice's strain energy, and discuss its implications for the mechanism of conduction. We also consider the vibrational densities of states of the inherent structures and test the possibility that an increase in the harmonic vibrational entropy upon defect formation stabilizes the superionic state. A mean-field model with an interaction term varying with the cube-root of the defect concentration describes the inherent structure defect populations well, and also reproduces the energy and entropy over a significant temperature range. However, a direct examination of the way in which the inherent structure energy depends on the defect concentration shows that this does not mean that the physical picture used to construct the mean-field free energy is correct.

1. Introduction

In a recent paper, called here paper I,[1] we showed that the dynamic and thermodynamic properties of fluorite-structured superionic crystals close to the superionic transition resemble those of supercooled liquids close to the glass transition. In these systems one ionic species forms a crystalline lattice,[2] while the other becomes progressively more mobile across the superionic transition, without a change in the crystal structure. The analogy between superionic and supercooled liquid is best seen by following the loss of mobility as the superionic is cooled from the melting point (where the conductivity has liquid-like values). The decrease in conductivity as the superionic transition is approached from above is similar to the structural arrest of a supercooled liquid as it is quenched into an immobile, glassy state. In paper I, we drew attention to the non-Arrhenius temperature dependence of the superionics' conductivities and diffusivities, and the existence of peaks in the heat capacities or, equivalently, a sharp decrease in the entropy on cooling to the immobile state. The transport coefficients and the entropy are connected by the Adam−Gibbs relation[3] over a significant range that includes the most non-Arrhenius variation of conductivity.

Apart from interest in understanding the superionics themselves, to which methods introduced for the glass transition may contribute, a reason for pursuing this analogy is that a description of the transport properties and thermodynamics of a disordered crystal naturally invokes the use of defects, which are readily defined by reference to the underlying crystal lattice. Defects are often invoked in theoretical models for the glass transition,[4−7] such as bond-defect models of the thermodynamics or kinetic Ising models of the cooperative aspects of the dynamics, despite the fact that they cannot be linked to the atomic arrangements in a disordered liquid. The superionic systems might therefore provide a direct, experimentally accessible realization of the scenario envisaged in these models. The superionic transition is simpler than the glass transition because it takes place in a system in thermal equilibrium, while the latter is a process of falling out of equilibrium. Also, the immobile, low-temperature state is the well-understood perfect crystal, whereas the glass is ill-condensed and strongly disordered. It is therefore of interest to understand the origin of the glass-transition-like phenomena of the superionic, since, in the supercooled liquids, these phenomena are sometimes regarded as peculiar to the transition to a strongly disordered and nonergodic state.

In paper I, we examined PbF_2 and CaF_2 in computer simulations; they exhibited very similar phenomenology but different degrees of "fragility". In the perfect fluorite structure, anions occupy all tetrahedral holes in the cubically close-packed cation sublattice. Defects were identified by partitioning the space in the crystal into tetrahedra and octahedra, with corners defined by the *instantaneous* positions of the ions on the (nondiffusing) cation lattice. We call empty tetrahedral sites "vacancies" and fluoride ions in octahedra of cations "interstitials". The number of defects identified by this procedure corresponds extremely well to the number of off-site anions found in refinements of diffraction experiments on PbF_2.[8] These simulated defects tend to cluster,[9] in the same manner as detected in diffuse scattering experiments.[10] Our attempt to relate the thermodynamic and transport properties to the number of these defects was partially successful (see paper I). We showed that CaF_2 and PbF_2 have the same dependence of entropy on the number of defects, despite the difference in the temperature dependence of their properties, but this entropy is *higher* than that of defects randomly assigned to lattice sites. There must be some other contributor to the entropy. At temperatures well below the superionic transition, where the number of defects is small, the diffusion coefficient of the ions is proportional to the number of defects, as would be anticipated from a simple defect-hopping picture of the ionic motion, but in the vicinity

† Part of the special issue "Hans C. Andersen Festschrift".

* Corresponding author.

10.1021/jp038026a CCC: $27.50
Published on Web 05/05/2004

of the transition, where the non-Arrhenius temperature dependence is pronounced, the diffusion coefficient increases more rapidly than the defect number. This suggests that interaction between the defects is promoting the ionic motion. The temperature dependence is captured by the Adam−Gibbs relationship over a significant range but, since we do not understand fully the dependence of the entropy on the defect number, this does not provide a route to a mechanism for the cooperativity which would link it to the defect interactions.

These considerations suggest a more fundamental look at the properties of the superionic crystals and their relationship to the degree of disorder by an attempt to characterize the nature of the "energy landscape". This approach has been very fruitfully applied to discuss the properties of supercooled liquids.[11] At low temperatures a supercooled liquid vibrates in potential-energy basins for long periods and moves rarely between them. It is this rare motion between basins that determines structural relaxation. Each basin may be represented by its local potential-energy minimum, or "inherent structure".[12,11] A sequence of inherent structures describes the dynamics better than the full trajectory[13] and, with vibrations removed, important processes are brought into focus. The thermodynamic properties of the supercooled liquids are largely determined by the number of these wells that are accessible for a given thermal history and by their vibrational properties. The entropy and internal energy of supercooled liquids have been reproduced, quantitatively, by counting the accessible basins and by measuring the vibrational entropy and energy in each of them.[11]

Each inherent structure for a superionic system may be characterized in terms of the defects it contains and their interactions. Although inherent structures can be found and counted for glass formers, and analyses of their structures have been made,[14,15] the task of understanding the energy landscape in the superionic case will be made easier by the crystalline matrix. We are ultimately interested in dynamics, but in this paper we mostly discuss thermodynamics and structure. Our final goal is a concrete physical picture leading from microscopic defect properties to macroscopic thermodynamic properties and transport coefficients.

Section 2 describes the methods we used to find the inherent structures and their properties from the simulations. The structures themselves and the tendency of defects to cluster are discussed in section 3. Section 4 describes the calculation of the harmonic vibrational properties of the inherent structures. In section 5 we collect the data obtained by sampling over a large number of inherent structures at each temperature and use them to deduce how the inherent structure energies and their harmonic vibrational entropies depend on the defect concentration. We discuss our results in more detail in section 6.

2. Methods

We use molecular dynamics simulations to generate configurations in the canonical ensemble,[16] and for the results of section 5.3 we use the isothermal−isobaric ensemble, with thermostats and barostats as described in refs 17 and 18. The details of the simulations have been given elsewhere: the calcium fluoride simulations[19] use a rigid-ion potential from reference 20, but the lead fluoride simulations permit dipolar polarization of both species.[9,21] All runs contained 324 ions. Most runs were nearly 10^6 steps of $\sim$0.5 fs long, but we stopped some much sooner, if all their inherent structures turned out to be the perfect crystal, for instance.

The inherent structures are obtained by selecting configurations from the MD trajectories and finding the local potential energy minimum. We use several steps of steepest-descent before calling a conjugate-gradients routine.[22] Once the steepest descent algorithm has trapped the system in a local minimum, the efficient conjugate-gradients method moves quickly to the actual minimum. The vibrational density of states and the harmonic parts of various properties of the inherent structure are found by numerically evaluating the dynamical matrix at the minimum and then calculating the normal modes of vibration.[23]

The method used to find the inherent structures for PbF_2 requires minimization of the potential energy with respect to the particle positions, with correct dipoles at all times. We use a conjugate-gradients linear solver to find the dipoles during the search for inherent structures.[24] This solver minimizes the potential energy with respect to the dipoles with all ions held fixed; since the potential energy is quadratic in the dipoles, this requires only the solution of linear equations. The conjugate-gradients method used for the inherent structures minimizes the potential energy with respect to the particle positions, with correct dipoles at all times.

3. Defect Clusters

We identify defects in the inherent structures in the way described in the Introduction. This definition differs from those used in previous works by Gillan[20] and Maier.[25] We will be interested in the relationship between the number of defects found in a molecular dynamics run at a given temperature, which we call "equilibrium defects", and those found in the inherent structures generated from the same MD configurations, the "inherent defects". The equilibrium defects are from an ensemble of configurations in thermodynamic equilibrium; the inherent structures are in mechanical equilibrium.

Four representative lead fluoride configurations are shown in Figure 1. The upper snapshots are from the molecular dynamics runs, just above and just below the heat-capacity maxima whose locations define the superionic transition. Interstitial fluoride ions are shown in green, vacancies are red, lead ions blue, and on-site fluorides are yellow. The bottom snapshots are the corresponding inherent structures, color-coded in the same way. On the left, the lead fluoride structures from below the heat-capacity peak illustrate the loss of some isolated defect pairs on minimization; that is, the interstitials and vacancies have recombined during the minimization process. The defect pairs that recombine easily are on adjacent sites and correspond to large-amplitude vibrations, which move ions into adjacent empty octahedra. Three clustered defects survive minimization even though they too are near vacancies. Without some sort of interaction, the presence of three defects so close together would be very unlikely, and it appears that this interaction also inhibits the recombination process since this configuration is a local energy minimum.

Both equilibrium and inherent configurations (right-hand structures in Figure 1) taken from just above the transition have many more defects, though the temperature is only 25 K higher. The clustering of defects in the inherent structure is now more pronounced. Almost two whole rows of fluoride ions are missing from their perfect crystal sites in the middle of the large cluster. In the equilibrium structure at 950 K defects are fairly evenly distributed through the cell, but those that do not survive minimization tend to be the isolated pairs.

There are four defects in a cluster near the top left corner of the lead fluoride inherent structure at 950 K; they form a tetrahedron around a vacancy. The cluster of three interstitials in the 925 K inherent structure is a fragment of a similar cluster.

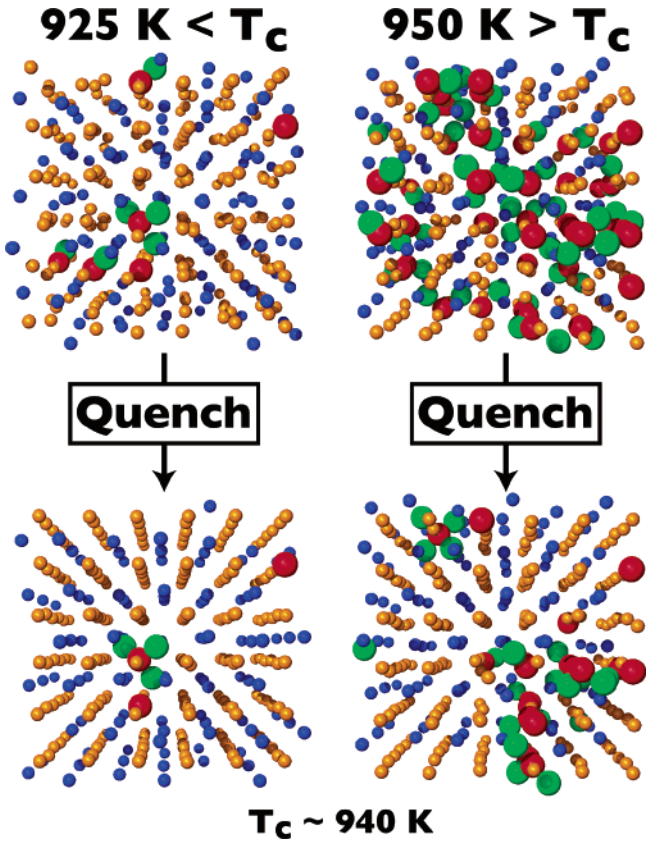

Figure 1. Snapshots showing structures from the molecular dynamics trajectories and the corresponding inherent structures. The yellow particles are on-site anions, the blue are lead ions, the green are interstitial fluoride ions, and the red are vacancies, i.e. the centers of empty tetrahedra. The upper configurations are taken from molecular dynamics runs, just below and just above the superionic transition. The lower configurations are the corresponding inherent structures, found by potential energy minimization from the top ones, as described in section 2. The cluster of four interstitials around a vacancy at the top left of the lead fluoride inherent structure at 950 K is that observed in doped lead fluoride at low temperature by Castiglione et al.[9] Note the periodic boundary conditions.

This tetrahedron of interstitials is the structure reported at much lower temperatures in simulations of PbF_2 doped with YF_3,[9] which introduces extra ("extrinsic") interstitials into the PbF_2 lattice. It was suggested that a similar structure was adopted by intrinsic interstitials above the superionic transition as for extrinsic ones at low temperature, but that thermal agitation made the intrinsic structure hard to see. These inherent structures confirm this suggestion.

Figure 2 shows the mole fractions of the two types of defects, equilibrium and inherent, for lead fluoride. There are some extra defects in the equilibrium structures, but the number of such defects seems not to increase much above the transition. Once clustering appears the two defect fractions grow at the same rate, suggesting that clusters of inherent defects emerge as the isolated equilibrium defects become more numerous and begin to interact. These isolated equilibrium defects below the transition are mostly lost on minimization, and so can be regarded as large-amplitude vibrations. This view is supported by the decay of collective defect-density fluctuations discussed in paper I, where, below the transition, the defect density decays inside one vibrational period. Above the transition, clusters of defects survive into the lead fluoride inherent structures, and again this is reflected in the time-correlation functions: decays of defect density resemble more those of a liquid and are much slower. The strong tendency of the defects to cluster above the

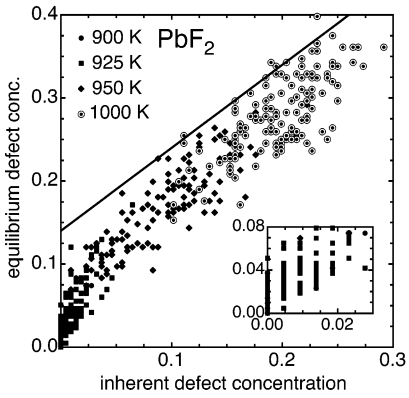

Figure 2. Mole fraction of fluorides that are outside their perfect-crystal tetrahedra for lead fluoride, i.e., the defect concentrations. The equilibrium defect concentrations are plotted against the same quantity for the corresponding inherent structures. Each point represents a point on a molecular dynamics trajectory and its corresponding inherent structure.

transition has a further signature in the dynamical properties. We noted in paper I that the ratio of the true conductivity to that calculated from the Nernst−Einstein relationship became substantially greater than one above the transition, indicating substantial correlations in the displacements of charged particles.

The conductivities of calcium fluoride and lead fluoride are similar at their transitions, as are the equilibrium defect concentrations. The many similarities between the two compounds suggest that the physical processes involved in the superionic system are essentially the same, though the calcium compound's transition is smoothed out over a much larger range of temperature. From this perspective it is surprising (and disappointing) that the relationship between the equilibrium and inherent defects found by implementing the procedures described above is found to be different for the two materials. In the early stages of the potential energy minimization to find the inherent structures, the two systems behave very similarly. But, whereas the PbF_2 then rapidly settles into what is found to be a true (local) minimum, containing several inherent defects, the CaF_2 minimization continues to evolve, progressively eliminating more and more defects. It is as if the interdefect interactions that stabilize local minima in PbF_2 are weaker in CaF_2 and do not frustrate a continued approach to a deeper energy minimum closer to the perfect crystal. The potential energy surface in CaF_2 seems to be dominated by smooth-bottomed, gently sloping valleys rather than local minima resembling those found in supercooled liquids. For this reason, we will discuss only the inherent defects for PbF_2 case in this work and return to a consideration of CaF_2 alongside other examples of superionic materials in a future publication.

3.1. Defect Density Profiles. To confirm the impression gained from the snapshots in section 3, of the sudden appearance of *clustered* inherent defects near the transition, we have constructed defect radial distribution functions (RDFs) as a measure of the average relationship between the positions of defects as a function of temperature. In Figure 3 we show the functions

$$\gamma_{NN}(x) = cg_{NN}(xa) = c[g_{II}(xa) + 2g_{VI}(xa) + g_{VV}(xa)] \quad (1)$$

$$\gamma_{ZZ}(x) = cg_{ZZ}(xa) = c[g_{II}(xa) - 2g_{VI}(xa) + g_{VV}(xa)] \quad (2)$$

where c is the mole fraction of vacant tetrahedral sites; $g_{ij}(r)$ is the partial radial distribution function for defect species i and j, where V denotes vacancies and I interstitials; a is the unit cell

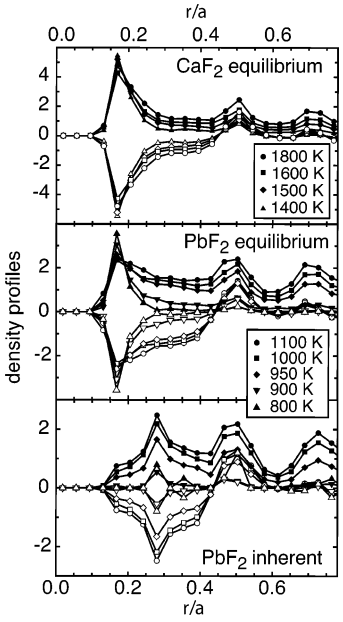

Figure 3. Curves giving the profile about a central defect of the defect-number density (filled symbols) and defect-charge density (empty symbols). They are combinations of the partial defect RDFs multiplied by the fraction of vacant fluoride sites, as described in section 3.1. The top and middle panels show these functions calculated from points on molecular dynamics trajectories, the bottom one shows them calculated from lead fluoride's inherent structure defects. Note the changes in both across the superionic transitions, at about 940 K in lead fluoride and 1450 K in calcium fluoride. The large first peak, which represents adjacent vacancy−interstitial pairs vanishes in the inherent structures.

length; and $x = r/a$. $\gamma_{NN}(x)$ is the defect-number density profile about a central defect, and $\gamma_{ZZ}(x)$ the corresponding defect-charge density profile. We choose these functions rather than the RDFs themselves because they permit display of all the profiles on one set of axes, and comparison of corresponding peaks as the cell expands with temperature. The shapes of these functions resemble those of a fluid of charged particles.

Consider first the upper two panes of Figure 3, where the density profiles for equilibrium defects in both fluorides are shown. Note first the value of γ_{NN} at large r. At the larger separations the peaks just reflect the crystal structure, and here γ_{NN} varies simply with the defect concentration. Both γ_{NN} and γ_{ZZ} have large first peaks below the transition, and they appear because defects are created in pairs of opposite charge, and indeed pairs with this separation are visible in Figure 1. The first peak, at the smallest interdefect separation at $x \sim 0.17$, arises from oppositely charged vacancy and interstitials, the next closest are the vacancy−vacancy and interstitial−interstitial distances, which give rise to the peaks at $x \sim 0.5$. There is a large change in the profiles across the superionic transition. The sharp first peaks broaden above the transition, and in both γ_{NN} and γ_{ZZ} the height of the first peak is *lower* at higher temperatures.

In the bottom part of Figure 3 the density profiles for inherent defects in lead fluoride are shown. Note that the concentrations of inherent defects are lower than those of equilibrium defects. The large first peak has disappeared, because closely spaced interstitial−vacancy pairs are likely to be annihilated on minimization (they are vibrations, not proper defects), but pairs a little further apart survive. The first peak in the inherent profiles coincides with the extra density appearing at the transition in both sets of equilibrium profiles. The separations at which this extra density appears are characteristic of the clusters.

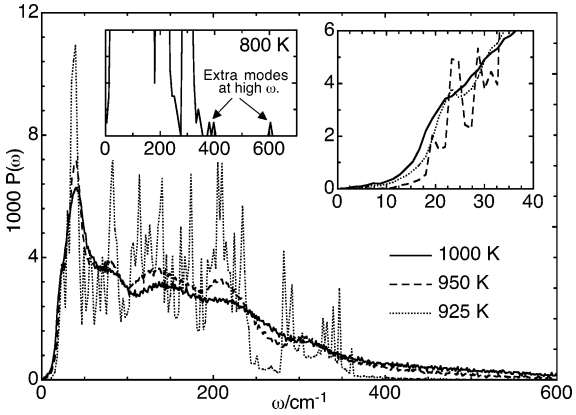

Figure 4. Vibrational density of states (DoS) calculated from the inherent structures of lead fluoride at three temperatures across the superionic transition. The left inset shows the DoS for a single inherent structure with a single defect from a run at 800 K. There are three new modes not present in the crystal at high frequency: these are the vibrations of the interstitial in its octahedron. Compare them to the long tail of high-frequency modes in the main plot, where there are more defects. The right inset shows a magnified version of the main plot, emphasising the increase in the DoS near 20 cm^{-1}, reminiscent of a similar feature found in glass formers, the boson peak. Overall, the inherent structure DoS resembles that discussed by Dederichs et al. for a defective crystal,[26] rather than that typical of a glass former.

Below the transition, equilibrium defect pairs vibrate into existence, giving rise to the first peak in the equilibrium defect distribution functions at $x \sim 0.17$, though very few inherent defects are found. This is the region where the time decay of defect density fluctuations, discussed in paper I, is dominated by phonons and the decay of defect density is fast. As the concentration of these defect pairs increases they begin to interact, and this interaction helps them survive the energy minimization to the inherent structure. That is why the inherent defect concentration varies more sharply at the transition. Above the transition where many of the inherent defects are present, the time decay of density fluctuations looks more like that of a liquid.

In the third panel of the figure, we show the density profiles for the *equilibrium* defects in CaF_2. We think it is significant that the equilibrium defect density profiles for calcium fluoride change in the same way as the lead fluoride ones across the transition, and that the extra density appearing at the transition coincides with the inherent profiles' main peak in the lead compound. From this perspective, PbF_2 and CaF_2 again look very similar, which further highlights the surprising difference in their inherent structures.

4. Vibrational Properties

One possible source of the increase in entropy that stabilizes the superionic state (discussed in paper I) is the change in harmonic vibrational entropy brought about by the rapid increase in the number of defects. Figure 4 shows the vibrational density of states (DoS) averaged over inherent structures for lead fluoride at three temperatures across the superionic transition. The vibrational density of states is found by evaluating the dynamical matrix at each inherent structure and then diagonalizing it to find the vibrational eigenvalues. The lowest temperature spectrum has the sharp structure we expect to find in a simulation of a crystal with periodic boundary conditions. The $3\times3\times3$ unit cells in the simulation cell permit sampling of only

a few wavevectors in the first Brillouin zone, and so we see sharp peaks in the DoS. As the system becomes increasingly disordered, due to the presence of more and more inherent defects, we expect the vibrational eigenstates to cease to be characterized simply by the wavevector and the eigenfrequencies to become more smoothly distributed. In fact, the transition between the sharply peaked, crystal-like DoS and a smooth more glass-like one is found to occur at the transition temperature.

The two important changes to the spectra at the transition are the appearance of a long tail of high-frequency modes and a small increase in the number of low-frequency modes, at about 20 cm^{-1}. These changes in the spectrum are consistent with ideas discussed some time ago by Dederichs.[26] He showed that the presence of an interstitial in a monatomic crystal would result in the appearance of new, localized low- and high-frequency modes. The left inset in Figure 4 is the DoS for a single inherent structure at 800 K, which happens to contain a single defect. It shows three extra high-frequency modes. These few anticipate the larger tail of modes in the higher temperature inherent structure DoS. Examination of the eigenvectors shows these are the vibration of the single interstitial in its octahedron, and involve very little motion of any other ions. If we assume that these modes are harmonic, we can calculate their amplitudes at 800 K and find them comparable to the size of the octahedron: such high amplitude motions must be highly anharmonic.

The extra modes at 20 cm^{-1} are reminiscent of the extra modes in glass-forming liquids at about this frequency, which are associated with the appearance of a boson peak in experimental spectra. Recent inherent structure calculations for a model of the fragile glass former ortho-terphenyl showed the loss of high-frequency modes and the appearance of low-frequency modes on moving to higher energy inherent structures.[27] These low-frequency modes entropically stabilize the high energy, more fluid states on heating. However, the increase in the DoS near 20 cm^{-1} shown in Figure 4 is small compared to those typical for glass formers, and, as we will see below, is not enough to produce an increase in the entropy compared to that calculated from the crystal-like DoS obtained from the inherent structures below the transition temperature.

5. Inherent Structures and Thermodynamic Properties

5.1. Energies and Harmonic Entropies. The lead fluoride inherent-structure energies are shown as a function of defect concentration in the top panel of Figure 5. The points obtained for inherent structures generated from different MD configurations at the same temperature are represented by the same symbols. The inherent structure energies increase with the temperature of the MD run from which they are generated, as is the case with the supercooled liquids. We have already seen that the number of defects increases with temperature. The variation of inherent structure energy could be compared to that seen in a glass-forming liquid, see, for instance, reference 28. The main difference is that in a supercooled liquid the rate at which the supercooled state has been prepared by cooling the normal liquid affects the energies of the populated inherent structures.

The straight lines in the upper part of Figure 5 are best fits. In a mean-field theory, the slopes of these lines would be estimates of the inherent defect creation energy per unit concentration. It is interesting to note that there is a substantial difference between the slopes obtained below and above the superionic transition temperature. In this mean-field viewpoint, the defect formation energy drops by about a factor of 10 across the transition.

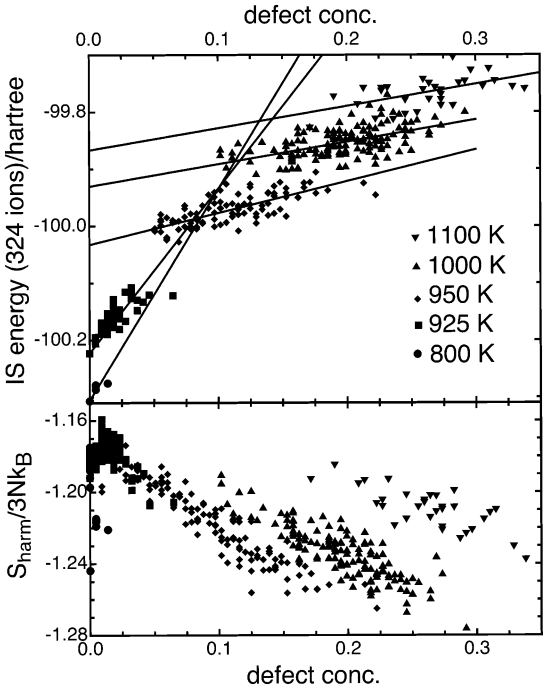

Figure 5. Inherent structure energy (top) and harmonic entropy (bottom) for lead fluoride versus the inherent defect concentration. Inherent structures obtained from MD runs at the same temperature as represented by the same symbol. The straight lines in the energy plot are fits to the points at each temperature discussed in the text. Only changes in the entropy are meaningful.

The intercepts of these lines with the vertical energy axis can be interpreted as the energy of the perfect lattice at the density appropriate to the simulation temperature under isobaric conditions. The energies found from this extrapolation are close to the lattice energies calculated directly for the perfect crystal at the lattice parameter appropriate to the isobaric simulation at the appropriate temperature, as discussed in paper I. We therefore see that the variation in lattice energy across the transition is significantly larger than the variation in energy directly associated with creation of the additional defect concentration in the expanded lattice. This then is the dominant energy opposing the transition to the superionic state.

The lower panel of Figure 5 shows the harmonic vibrational entropies for the same structures. The harmonic entropy is calculated from the vibrational eigenfrequencies discussed above using[11]

$$\frac{S_{\mathrm{harm}}}{3Nk_{\mathrm{B}}} = -\int_0^\infty \mathrm{d}\,\omega P(\omega)\log(\beta\hbar\omega) + \ldots \qquad (3)$$

where the integral is the average of $\log(\beta\hbar\omega)$ over the density of vibrational states, and the dots denote terms that are not important because we are interested only in changes in entropy. There is a remarkable *decrease* in the harmonic entropy with defect creation at each temperature. The small increase from one temperature to the next is due entirely to the part of the harmonic oscillator entropy $-\log\,\beta$. In other words, it is not due to the appearance of defects and would be present in any crystal. The positive contribution to the entropy arising from the defect-induced low-frequency modes, seen in Figure 4, is outweighed by the negative contribution due to the additional high-frequency modes. We reiterate the point made in paper I that the configurational entropy estimated by randomly assigning *equilibrium* defects to lattice sites was *lower* than the observed entropy change across the transition. Since the number of

inherent defects is smaller than the number of equilibrium defects, the configurational entropy associated with randomly placed inherent defects must also be smaller, and, since the harmonic entropy arising from defect formation is now seen to be negative, there remains a large contribution to the entropy whose origin we have not yet identified. In studies of supercooled liquids, the configurational entropy found by actually counting the number of inherent structures and the harmonic vibrational entropy account for most of the entropy, so that the equation of state may be predicted from the inherent structures.[11] We have not attempted such a calculation, since we would need to sample far more inherent structures in order to make a better estimate of the configurational term. As we shall see, we can learn a great deal from the energies of the inherent structures alone.

5.2. Mean-Field Models of the Inherent Defects. We turn now to the possibility that the temperature dependence of the inherent defect concentration in lead fluoride may be described by a mean-field model. Our aim is in part to evaluate the ability of a cube-root model of the defect free-energy to describe thermodynamic properties at the superionic transition, but also to illustrate how much can be learned from the detailed microscopic information provided by the inherent structure calculations. Mean-field models of superionics resemble the "bond-lattice model" of supercooled liquids,[4] with the defects in the crystal lattice replacing broken "bonds" in, for example, an amorphous tetrahedral network. In paper I, we analyzed the equilibrium defects with a variety of mean-field models and concluded that the "cube-root model"[25] fits best, so we consider that model here.

The substantial scatter about the straight-line fits of the inherent structure energies to the number of defects at each temperature (Figure 5) might make one wonder if a mean-field model could ever describe the energetics correctly. This scatter arises from the variation in energy due to differences in the way a given number of defects are arranged. However, we have now seen that a large part of the inherent structure energy is lattice energy and, on the scale of the *total* inherent structure energy variation with defect number, the fluctuating part that depends on the specific defect configuration becomes relatively small.

The cube-root model is described in more detail in paper I and in reference 25. It expresses the free energy in the form

$$\beta g = (\beta h - s)c - s_r(c) + \beta g_{ex}(c) \quad (4)$$

$$g_{ex}(c) = \int_0^c \mathrm{d}x\, \mu_{ex}(x) \quad (5)$$

where h is a defect creation enthalpy, s is a defect creation entropy, and $\mu_{ex}(c) = -Jc^{1/3}$ is the excess chemical potential that represents defect interaction. The entropy for randomly placed defects is

$$s_r(c) = \alpha \log \alpha - 2c \log c - (1 - c) \log(1 - c) - (\alpha - c) \log(\alpha - c) \quad (6)$$

where $\alpha = 1/2$ is the maximum possible defect fraction. This entropy expression is obtained by randomly assigning the interstitials to the lattice of octahedral sites (assumed to be at most singly occupied), and randomly assigning the vacancies to the lattice of tetrahedra. The straightforward interpretation of this free energy is as that of a set of weakly interacting (hence randomly placed) defects on an otherwise unchanged lattice. It is not at all clear that this will represent the superionic systems

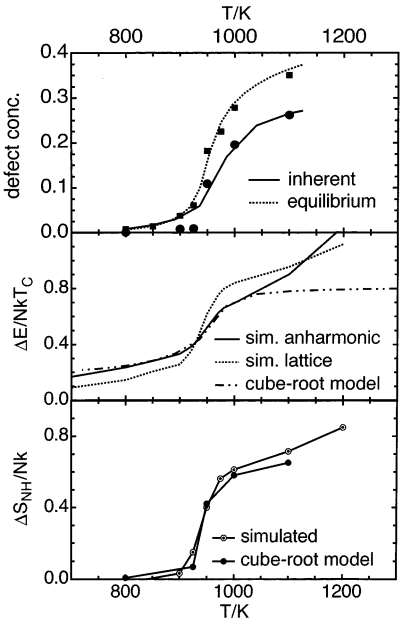

Figure 6. (top plot) Cube-root model fits to equilibrium (squares and dotted line) and inherent (circles and solid line) defect concentration, for which the parameters are given in Table 1. The lower two plots show predictions of the cube-root model for the temperature variation of anharmonic energy (middle) and anharmonic entropy (bottom) in lead fluoride. The parameters were obtained by fitting to the inherent defect concentration but reproduce the energy and entropy over a fair range of temperature.

TABLE 1: Parameters Found by Fitting the Cube-Root Model[25] to the Variation of Defect Concentration with Temperature for Lead Fluoride: Both Fits Are Shown in Figure 5

	h/kT_c	s/k	J/h
equilibrium	13.7	3.7	1.0
inherent	10.8	0.21	1.4

near and above the transition, where, as we have seen, the lattice energy is a substantial contributor to the enthalpy change across the transition and the defects are not randomly arranged.

The cube-root model fits to the concentration of inherent and equilibrium defects are shown in the top panel of Figure 6. The cube-root model fits the equilibrium defect concentrations very well, as we saw in paper I, but cannot quite reproduce the sharp variation of inherent defect concentration across the transition. Still, the fit is reasonable. The values of the parameters for the inherent concentration fit are quite different from those obtained from the equilibrium defects in paper I. The defect enthalpy is a little smaller for the inherent defect fit, and the interaction a little stronger, as we would expect for a sharper variation in the defect concentration. The defect entropy is much smaller. Both sets of parameters are given in Table 1. More importantly, the parameter, h, supposedly a defect creation enthalpy, is much larger than the slopes of any of the lines in Figure 5.

Figure 6 also shows the energy and entropy from the lead fluoride simulations compared to the *predictions* of the cube-root model with the parameters obtained from the fits to the inherent structure concentrations. The energy and entropy of the system are well represented across a significant range of temperature near the transition, of about 200 K. Although the fit of the cube-root model to the actual defect concentration is not as good as for the equilibrium defects, the application to the inherent defects agrees with the thermodynamics much better. It reproduces the observed behavior of the entropy and

energy quite well, in contrast to the equilibrium defect case where these quantities are overestimated (*cf.* paper I).

The inherent structure energies at each temperature in Figure 5 are roughly linear in the defect concentration over quite a wide range and provide no justification for a direct mean-field interaction between inherent defects in lead fluoride. The only effect of interactions appears to be the fluctuation of the energy with defect configuration, which is small compared to the total inherent structure energy. We also know that the fitted parameter, h, does not agree with the defect creation energies estimated from these slopes of the inherent structure energies (see Figure 5) versus defect number and that these slopes are strongly temperature dependent. We conclude that although the enthalpic part of the cube-root model free energy, $hc - (3/4)Jc^{4/3}$, fits the inherent structure energies satisfactorily, the usual interpretation of the parameters is flawed. The success of the cube-root model arises because the terms linear in c and $Jc^{4/3}$ in the enthalpy term in the free energy combine to incorporate the change in lattice energy of the perfect crystal as it expands.

The physical significance of the entropy terms in the cube-root model is also suspect. They include s_r, which would be the entropy of randomly arranged defects, and a defect creation entropy. We know that the defects form clusters and are certainly not randomly arranged. It is hard to see how clustering could produce an entropy contribution linear in the concentration. Again, it seems that the quality of fit of this function to the entropy is fortuitous.

The ability of the cube root model to describe the defects and thermodynamic properties of the superionic system in a consistent way is a big success. However, the microscopic examination we have undertaken suggests that the underlying physical picture of a weakly interacting gas of defects is not well-founded, and should not be used as a basis on which to understand other properties and, in particular, the dynamics.

5.3. Role of Lattice Strain in Defect Formation. Figure 5 provides strong evidence that the lattice expansion is strongly correlated with the number of defects, but we would like to confirm this directly from the molecular dynamics runs. We have examined the correlation between fluctuations in defect concentration (c), potential energy (U), and cell length (L) in a constant-pressure simulation. For the defect concentration we used the equilibrium defects. The difference between the inherent and equilibrium defects is not critical for lead fluoride, since, in the region of the transition and above, their concentrations are closely related.

We define a dimensionless measure of correlation between two variables,

$$R_{AB} = \frac{\langle AB \rangle}{\sqrt{\langle A^2 \rangle \langle B^2 \rangle}} \tag{7}$$

where A and B are two of the three variables U, L, and equilibrium defect concentration, c. Brackets $\langle \cdot \rangle$ denote averaging over the isothermal−isobaric ensemble implemented as described in section 2. Figure 7 shows these three functions for CaF_2 and PbF_2. For lead fluoride, all three variables become much more correlated as the transition is approached from above. The correlation is weaker for calcium fluoride, but the correlation between cell size and defect concentration stands out more, with the other two functions varying little over the whole range of temperature. For both materials the cell size and defect concentration are particularly strongly correlated in the region of the transition. The peaks in the heat capacity and compressibility appear at the transition because the fluctuations have become large, as the system moves between superionic and normal states. In this region cell expansion goes with defect creation because otherwise defect creation would be too energetically expensive. At higher temperatures the fluctuations cease to be correlated because the lattice is in its expanded state almost all the time. Defects need not wait for expansion before they appear. This supports our conclusion in section 5 that lattice distortion is an important influence on defect creation.

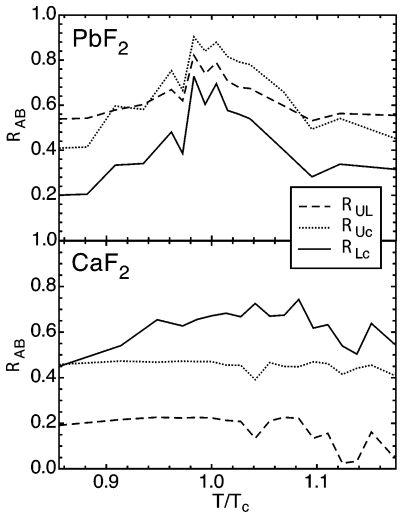

Figure 7. Correlations between fluctuations in the potential energy, box size, and defect concentration, in constant-pressure simulations, described in section 5.3. The correlation between box length and defect concentration is particularly strong near the transition for both materials.

The model for the melting of face-centered-cubic metals given by Granato has a free energy that depends not only on the crystal density but also on the bulk modulus and shear modulus, and their pressure derivatives.[29] The elastic moduli are related to fluctuations in the strain field. We considered above only fluctuations in density, but plan to examine other strains. The fluctuations in the defect concentration are related to their chemical potential, and the fluctuations in strain to the appropriate elastic constant, the isothermal compressibility in this case. The cross correlation of cell size and defect concentration, R_{Lc} in Figure 7, is then a measure of the effect of pressure on the concentration of defects or the effect of defect creation on the pressure. If the pressure is increased, the relative change in defect concentration is greatest near the transition because the system is compressed out of the superionic state. It is possible to extend the results in Figure 7 and calculate the defect chemical potential and its connection to the various elastic constants. The probable mechanism for the connection is that the creation of one defect softens the lattice so that another can form more easily. Clustering will play a role here, if the mechanism for defect interaction suggested above is correct.

6. Summary and Discussion

We have shown that inherent structures that contain large numbers of clustered defects exist in lead fluoride above its superionic transition temperature. As it is cooled from its melting point, the average energy of the populated inherent structures decreases along with the fluoride ion mobility. A similar process takes place in a supercooled liquid (see for example references 28 and 11), with the added complication that the inherent structures chosen by the fluid depend on the rate at which the supercooled liquid has been cooled.

Some analyses of the energy distributions of glassy inherent structures have examined their relationship to the atomic

configurations,[14,15] but that task is much easier for the superionic systems because of the crystalline matrix, which allows the inherent structures to be characterized by the number of defects they contain. We see from the inherent structure energies that much of the anharmonic energy variation across the superionic transition is lattice energy, associated with an expansion of the lattice, and the defect creation energy drops sharply (see Figure 5). There is a sharp contrast between this lattice-governed change in thermodynamic properties in the vicinity of the transition and the natural picture used to discuss ionic motion in a low-temperature crystal of weakly interacting defects in an otherwise undistorted lattice. Nevertheless, we have seen that a generalization of the low temperature picture, in which the free energy of a set of randomly positioned defects contains a mean-field interaction term involving the cube-root of the defect concentration,[25] reproduces the defect concentration and the enthalpy and entropy, but the physical interpretation of the various terms in this cube-root model is not supported by the direct examination of the energetics of the defects and their interaction. We have still to examine fully how the inherent structures can be used to calculate the entropy of the system, in the manner already achieved for supercooled liquids.[11] However, the estimates we have made of the change in harmonic vibrational entropy associated with defect formation show that this does not explain the large increase in entropy across the transition.

The significance of the lattice energy to the transition, and an examination of the positional correlations between the defects, leads us to propose a mechanism for the clustering of the defects. Four defects close together around a vacancy cause much less distortion of the lattice than randomly distributed defects. If the energy required to uniformly expand the lattice is the main cost that must be overcome across the transition, then it may be that the need to minimize the energy cost of nonuniform distortion is behind defect clustering. The cluster still has a stabilizing entropy associated with its position, orientation, and the positions of the three remaining vacancies, and there is also the extra entropy from the lowering of the density. It is tempting to identify these clusters with the source of cooperativity that gives the superionic transition dynamical features in common with the glass transition in a fragile, supercooled liquid, and further work will be directed toward further clarifying this connection. We have already been able to indicate how the clusters influence the relaxation of the intermediate scattering function of the superionic system and affect the conductivity by causing it to increase above the Nernst−Einstein value.

Motion of a fluoride ion from the crystal lattice to the interstitial lattice involves the creation of a defect pair. The mobility of a chosen ion depends on the number of nearby defects, and we have already seen in paper I that the mobility has a faster-than-linear dependence on the defect concentration above the transition. This picture resembles the kinetic Ising models mentioned in section 1, and we can anticipate dynamical consequences from the defect clustering similar to those predicted in these models. In the Kob−Anderson model,[6] for example, a lattice gas is augmented with a dynamical constraint that a particle may jump to an empty neighboring site only if it has m or fewer occupied neighbor sites. Our system has no such constraints; though an ion can only move if at least one neighbor site is vacant, there are no "jammed" configurations, and the system is always ergodic. The clustering of inherent defects must affect the transport of charge. Regions with more disorder will permit more jumps from site to site than crystalline regions, for the reasons noted above. This means that there are defect-rich regions of the crystal that are more mobile than others (*cf.* Figure 1). This is a type of dynamical heterogeneity, whose origin is the defect interactions and not imposed constraints.

Though the number of equilibrium defects along the molecular-dynamics trajectory in CaF_2 is similar to that in PbF_2, many more are lost on minimization to the inherent structure. In almost all other ways the transitions in the two materials are very similar, though calcium fluoride's is at a higher temperature and less sharp. We have shown another piece of evidence for a similar mechanism in calcium fluoride in the pair correlations in the equilibrium defect density. There is a qualitative change across the transition in lead fluoride and a similar but weaker change in calcium fluoride. In lead fluoride, the new features that appear in the pair correlations at the transition can be clearly identified with the clusters of defects seen in the inherent structures: similar defect clusters are found in CaF_2, but many are annihilated during the energy minimization to the inherent structure. It may be simply that our minimization algorithm is "too good" and skips over the local minima in the CaF_2 case, but it is more likely to be an aspect of the smoother transition. That is, we have not yet examined a sufficiently wide range of temperatures to find inherent structures with a high number of defects, like those found in PbF_2.

The superionic transition can be regarded as the result of an opening out of the energy landscape. It is possible that the energy landscape of calcium fluoride broadens out just as that of lead fluoride but does not develop well-defined minima. We know already that the two energy landscapes have much in common: in paper I we showed that the two models have the same dependence of total entropy on equilibrium defect number across the transition. This opening out would provide the entropic drive to the conducting state, though in the inherent structure scheme the entropy would be largely anharmonic vibrational rather than largely configurational. The presence of well-defined minima in PbF_2 makes interpretation easier, but the energy landscape would still be a useful idea if they are absent.

References and Notes

(1) Gray-Weale, A.; Madden, P. A. *J. Phys. Chem. B* **2004**, *108*, 6624.
(2) Chandra, S. *Superionic Solids: Principles and Applications*; North-Holland: Amsterdam, 1981.
(3) Adam, G.; Gibbs, J. H. *J. Chem. Phys.* **1965**, *43*, 139.
(4) Moynihan, C. T.; Angell, C. A. *J. Non-Cryst. Solids* **2000**, *274*, 131.
(5) Fredrickson, G. H.; Andersen, H. C. *Phys. Rev. Lett.* **1984**, *53*, 1244.
(6) Kob, W.; Andersen, H. C. *Phys. Rev. E* **1993**, *48*, 4364.
(7) Berthier, L.; Garrahan, J. P. *J. Chem. Phys.* **2003**, *119*, 4367.
(8) Goff, J. P.; Hayes, W.; Hull, S.; Hutchings, M. T. *J. Phys.: Condens. Matter* **1991**, *3*, 3677.
(9) Castiglione, M. J.; Madden, P. A. *J. Phys.: Condens. Matter* **2001**, *13*, 9963.
(10) Hutchings, M. T.; Clausen, K.; Hayes, W.; Kjems, J. K.; Schnabel, P. G.; Smith, C. *J. Phys. C: Solid State Phys.* **1984**, *17*, 3903.
(11) La Nave, E.; Mossa, S.; Sciortino, F. *Phys. Rev. Lett.* **2002**, *88*, 225701.
(12) Sastry, S. *Nature* **2001**, *409*, 164.
(13) Doliwa, B.; Heuer, A. *Phys. Rev. E* **2003**, *67*, 031506.
(14) Perera, D. N.; Harrowell, P. *J. Non-Cryst. Solids* **1998**, *235*, 314.
(15) Schroder, T. B.; Sastry, S.; Dyre, J. C.; Glotzer, S. C. *J. Chem. Phys.* **2000**, *112*, 9834.
(16) Rapaport, D. C. *The Art of Molecular Dynamics Simulation*; Cambridge University Press: Cambridge, 1997.
(17) Tuckerman, M. E.; Martyna, G. J. *J. Phys. Chem. B* **2000**, *104*, 159.
(18) Tuckerman, M. E.; Martyna, G. J. *J. Phys. Chem. B* **2001**, *105*, 7598.
(19) Dent, A.; Wilson, M.; Madden, P. A. *Solid State Ionics* **2004**, *167*, 73.
(20) Gillan, M. J. *J. Phys. C: Solid State Phys.* **1986**, *19*, 3391.

(21) Castiglione, M. J.; Wilson, M.; Madden, P. A.; Grey, C. P. *J. Phys.: Condens. Matter* **2001**, *13*, 51.
(22) Press, W. H.; Teukolsky, S. A.; Vetterling, W. T.; Flannery, B. P.; *Numerical Recipes in C++*, 2nd ed.; Cambridge University Press: Cambridge, 2002.
(23) Ribeiro, M. C. C.; Wilson, M.; Madden, P. *J. Chem. Phys.* **1998**, *109*, 9859.
(24) Golub, G. H.; Loan, C. F. V. *Matrix Computations*, 3rd ed.; Johns Hopkins University Press: Baltimore, London, 1996; chapter 10, p 508.
(25) Zimmer, F.; Ballone, P.; Parrinello, M.; Maier, J. *Solid State Ionics* **2000**, *127*, 277.
(26) Dederichs, P. H.; Lehmann, C.; Scholz, A. *Phys. Rev. Lett*. **1973**, *31*, 11.
(27) La Nave, E.; Mossa, S.; Sciortino, F. *Phys. Rev. Lett*. **2002**, *88*, 225701.
(28) Sastry, S.; Debenedetti, P. G.; Stillinger, F. H. *Nature* **1998**, *393*, 554.
(29) Granato, A. V. *Phys. Rev. Lett*. **1992**, *68*, 974.